Journal of Molecular Structure 1150 (2017) 8–20

Contents lists available at ScienceDirect

Journal of Molecular Structure

journal homepage: http://www.elsevier.com/locate/molstruc

A structural and spectroscopic study on carquejol, a relevant constituent of the medicinal plant *Baccharis trimera* (Less.) DC. (Asteraceae)

Manuel Minteguiaga [a, b], Eduardo Dellacassa [b], Maximiliano A. Iramain [c], César A.N. Catalán [a], Silvia Antonia Brandán [c, *]

[a] INQUINOA-CONICET, Instituto de Química Orgánica, Facultad de Bioquímica, Química y Farmacia, Universidad Nacional de Tucumán, Ayacucho 471, T4000INI, San Miguel de Tucumán, Tucumán, Argentina
[b] Laboratorio de Biotecnología de Aromas, Departamento de Química Orgánica, Facultad de Química, Universidad de la República, General Flores 2124, Montevideo, 11800, Uruguay
[c] Cátedra de Química General, Instituto de Química Inorgánica, Facultad de Bioquímica, Química y Farmacia, Universidad Nacional de Tucumán, Ayacucho 471, T4000INI, San Miguel de Tucumán, Tucumán, Argentina

ARTICLE INFO

Article history:
Received 23 May 2017
Received in revised form
17 August 2017
Accepted 18 August 2017

Keywords:
Carquejol
Baccharis trimera
Vibrational spectra
Molecular structure
Force field
DFT calculations

ABSTRACT

Carquejol and its acetate are monoterpenoids based on the rare *o*-menthane skeleton and distinctive components of the essential oil from *Baccharis trimera*. Carquejol was characterized by using Fourier Transform infrared (FT-IR) and Raman (FT-Raman), Ultraviolet–Visible (UV–Visible), Electronic Circular Dichroism (ECD), Mass, Hydrogen and Carbon Nuclear Magnetic Resonance (^{1}H and ^{13}C NMR) and 2D ^{1}H–^{1}H gCOSY, ^{1}H–^{13}CgHSQC, ^{1}H–^{13}CgHMBC spectroscopies. Due to the chirality of this monoterpenoid, six different structures were analysed, of which only four showed higher populations and minimal energies. The natural bond orbital (NBO), atoms in molecules (AIM), Merz-Kollman (MK) charges, molecular electrostatic potentials (MEP) and frontier orbitals studies were performed in order to evaluate their structural, electronic, topological and vibrational properties. All calculations were performed by using the hybrid B3LYP method and the 6-31G* and 6-311++G** basis sets. The comparison of the experimental ECD spectra with the corresponding theoretical ones confirm the (4S,5R) configuration assigned to carquejol. The force fields for the most stable configurations were computed by using those two levels of theory and the complete vibrational assignments for the two conformations of carquejol are reported. The different orientations and directions of the dipole moments of the two structures and the proximity in the nucleophilic indexes with those reported for other terpenes could justify in part the potential biological properties reported for carquejol. The MEP surfaces for both structures reveal that the nucleophilic and electrophilic sites of higher reactivity are principally centred on the OH groups.

1. Introduction

Carquejol, IUPAC name 5-methylidene-6-prop-1-en-2-ylcyclohex-2-en-1-ol, is the oldest member of monoterpenoids based on the rare *o*-menthane skeleton. Carquejol together with carquejyl acetate are distinctive components of the essential oil obtained from aerial parts of *Baccharis trimera* (Less.) DC (syn. *B. genistelloides* Pers.)(Asteraceae), a medicinal plant commonly known as carqueja that grows wild in southern Brazil, Uruguay, Paraguay and northeastern Argentina. Infusions and decoctions of this plant are used for the treatment of gastrointestinal, hepatic and renal disorders, diabetes, rheumatism, poor blood circulation and inflammatory processes [1–11]. The secondary metabolite chemistry of carqueja has been investigated by several authors, the main groups of compounds identified being mono- and sesquiterpenoids in the essential oil [7,12] and flavonoids, polyphenols, tannins, diterpene lactones and saponins in extracts of different polarities [2–12]. Several of the isolated products exhibited remarkable therapeutic properties. For instance, the saponins present in the butanol extract showed strong anti-inflammatory and analgesic activity [3]; a clerodane type diterpene isolated from the ethyl

* Corresponding author.
E-mail address: sbrandan@fbqf.unt.edu.ar (S.A. Brandán).

http://dx.doi.org/10.1016/j.molstruc.2017.08.068
0022-2860/

acetate fraction of aerial parts produced full inhibition of haemorrhage and proteolytic activity caused by *Bothrops* sp. snake venom [4] whilst the essential oil showed promising schistosomicidal activity against the trematode species *Schistosoma mansoni* [11].

From chemical point of view carquejol is a monoterpene alcohol belonging to the *o*-menthane series that structurally has two asymmetric carbons and, for this reason, four stereoisomers (two pairs of enantiomers) are possible. On the other hand, it is recognized that the chirality of a drug is strongly related to its biological or pharmacological activities. This way, to identify carquejol by means of the vibrational spectroscopy it is necessary first to analyse all the possible structures in order to find the most stable theoretical configuration, that is the most stable energetically and, besides, to know if only a single or both enantiomers are present in the natural alcohol. Hence, the aims of this work were (i) to perform a structural theoretical investigation on the four possible stereostructures of carquejol based on the DFT calculations and taking into account the experimental structure and chirality reported for the natural compound [13], (ii) to characterize completely natural carquejol by using the experimental infrared, Raman, ^{1}H NMR, ^{13}C NMR, UV–Visible and ECD spectra and then, (iii) to perform the complete assignments of their vibrational spectra. With these purposes, the optimizations of the different structures and the calculations of the structural properties for the most stable configurations were performed using the hybrid B3LYP method together with the 6-31G* and 6-311++G** basis sets [14,15]. Thus, the Natural bond orbital (NBO) [16] and atoms in molecules (AIM) calculations [17,18] were used to compute atomic charges, molecular electrostatic potentials, bond orders, donor-acceptor interactions energy and, the topological properties such as, the electron density distribution, $\rho(r)$ and the Laplacian values, $\nabla^2\rho(r)$ [17]. Later, the predicted infrared, Raman, ^{1}H NMR, ^{13}C NMR and UV–Visible spectra using the two levels of theory were compared with the corresponding experimental ones and, afterward, the assignments of all the bands observed in these spectra were performed. Here, in order to perform the complete vibrational assignments of the most stable conformations of carquejol the normal internal coordinates and the Scaled Quantum Mechanical Force Field (SQMFF) methodology [19] were used together with the Molvib program [20] to compute the force fields with both basis sets. Taking into account the potential biological and pharmacological activities of this attractive component of carqueja essential oil, the reactivities and behaviours of all stable conformations were predicted by using the frontier orbitals and some descriptors reported in the literature [21–25]. Here, some structural properties were compared with those reported for other terpenes [26–28] while the gap values and the descriptors were compared with the reported for some compounds with different biological activities [24,29].

2. Experimental

2.1. Plant material

Aerial parts of *Baccharis trimera* (Less.) DC. were randomly collected at blooming stage (March 2016) in '*Estación Porvenir*' (32°21′56,5″S; 57°54′02,1″O), Paysandú Province, Uruguay. A voucher specimen was deposited at the 'Arechavaleta' Herbarium, Facultad de Química, Uruguay (MVFQ, UdelaR; M. Minteguiaga 4420); species identification was performed by Prof. E. Alonso-Paz.

2.2. Extraction of the essential oil and isolation of compounds

Fully air-dry plant material (30 Kg) was extracted in a pilot steam distillation unit (Eysseric Company, Nyons, France) at Agricultural Research National Institute INIA '*Las Brujas*' (Rincón del Colorado, Canelones province, Uruguay). In order to preserve the oil (approximately 45 mL), anhydrous sodium sulfate and butylated hydroxytoluene (Sigma-Aldrich) were added immediately after the extraction process. Then, the oil was stored in an amber flask at −4 °C until chemical analyses. The oil was characterized by carquejyl acetate (71,4%) and carquejol (0,5%) according to GC-MS analysis.

2.3. Carquejyl acetate

The essential oil was column chromatographed over Silica gel (Merck, 230–400 mesh; 530 g) with hexane-ethyl acetate 96:4 as elution solvent to give 105 fractions which were monitored by TLC. Fractions showing a single spot corresponding to carquejyl acetate were reunited and the solvent evaporated in vacuo (rotavap) to yield carquejyl acetate (5.78 g, purity 96.8% by GC). Chiral analysis using a capillary column CycloSil B showed that both carquejol and carquejyl acetate from *B. trimera* were enantiomerically pure.

2.4. Carquejol

Carquejyl acetate (12.90 g; 67 mmol) was saponified following the procedure described in Ref. [30] to yield crude carquejol (9.26 g, 92%) which was column chromatographed over Silica gel (Merck, 230–400 mesh; 320 g) with hexane-ethyl acetate mixtures of increasing polarity (96:4, 96:5 and 94:6) to yield 8.15 g of pure carquejol (purity >99.8% by GC) as crystalline needles, mp 38-39 °C. UV (*n*-hexane) λ_{max} (log ε) 208 nm (3.78). EI-MS (70 eV); *m/z* (%) $[M]^{+\bullet}$ 150 (1.7), 149 (1.5), 135 (62, $[M-CH_3]^+$), 133 (16, $[M-OH]^+$), 117 (45, $[M-CH_3-H_2O]^+$), 115 (17), 107 (44), 95 (23), 94 (49), 93 (24), 92 (17), 91 (97), 81 (20), 79 (100, $[C_6H_7]^+$) (RDA fragment −H), 77 (56), 70 (23,$[C_4H_6O]^{+*}$), 65 (23), 55 (16), 53 (17), 51 (16), 41 (24) (See Fig. S16). ^{1}H NMR (200 MHz, $CDCl_3$) (See Fig. 2) δ5.87 (1H; ddtd, 9.9, 3.2, 2, 0.4 Hz, H-4), δ 5.74 (1H; dtdd, 9.9, 3.3, 1.5 and 0.4 Hz, H-5), δ 5.24 (1H; m, fine splitting, H-9b), δ 5.04 (1H; quint, 1.4 Hz, H-9a), δ 4.97 (1H; q, 1.4 Hz, H-7b), δ 4.92 (1H; s br, H-7a), δ 4.41 (1H; m, H-3), δ 3.14 (1H; d br, 4.7 Hz, H-2), δ 2.89 (1H; d with fine splitting, 19.7 Hz, H-6b), δ 2.77 (1H; d with fine splitting, 19.7 Hz, H-6a), δ 1.87 (1H; d, 10.3 Hz, O–H), δ 1.78 (3H; dd, 1.4 and 0.7 Hz, Me-10) (Fig. 2).^{13}C NMR (50 MHz, $CDCl_3$) δ143.2 (C; C-1), 142.4 (C; C-8), 130.8 (CH; C-4), 128.1 (CH; C-5), 112.6 (CH_2; C-9), 111.6 (CH_2; C-7), 68.8 (CH; C-3), 54.3 (CH; C-2), 33.1 (CH_2; C-6), 23.8 (CH_3; C-10) (Fig. 3 and Fig. S11). IR and Raman spectra are shown in Fig. 4. Studies on the pharmacology [31a] and toxicity [31b] of carquejol are available. There is also a patent for preparing carquejol from carqueja essential oil [32].

2.5. General experimental procedures

NMR spectra were acquired on a Bruker instrument at 200 MHz (^{1}H) and 50 MHz (^{13}C). All spectra were recorded in $CDCl_3$ with the solvent used as an internal reference (δ_H 7.26; δ_C 77.3, 77.0, 76.7). 2D NMR spectra (^{1}H–^{1}H gCOSY, ^{1}H–^{13}C gHSQC, ^{1}H–^{13}C gHMBC) were acquired using standard Bruker programs. GC-MS analysis: Mass spectra were recorded on a 5973 Hewlett Packard selective mass detector coupled to a Hewlett Packard 6890 GC using HP-5MS (5% phenylmethylsiloxane) capillary column (30 m × 0.25 mm i.d.; 0.25 mm film thickness). The injector, GC-MS interphase, ion source and selective mass detector temperatures were maintained at 250 °C, 275 °C, 280 °C and 150 °C, respectively; ionization energy, 70 eV; injection size: 0.1 μL (10% solution in ethyl acetate) (split mode). Helium was used as carrier gas at a flow rate of 1.0 mL min^{-1}. The oven was programmed as follows: 50 °C (1 min), 50-100 °C at 1.0 °C min^{-1}, 100-150 °C at 2 °C min^{-1}, 150-270 °C at

10 °C min^{-1}, and then kept at 270 °C (5 min). In order to establish the enantiomeric distribution of natural carquejyl acetate and natural carquejol, a chiral selector capillary column CycloSil-B 30%-(2,3-di-*O*-methyl-6-*O*-tertbutyl-dimethyl)-β-cyclodextrin in DB-1701 (Agilent Technologies) (30 m × 0.25 mm i.d. × 0.25 μm film thickness) was used. The temperature program optimized to separate monoterpene enantiomers was as follows: 65 °C (1min), 65–100 °C at 1 °C min^{-1}, 100 °C (1min), 100–150 °C at 2 °C min^{-1}, 150–220 °C at 10 °C min^{-1}, 220 °C (3 min).

All chromatographic data were recorded and processed by ChemStation® software (Agilent Technologies). Column chromatography and TLC were performed using, Silica gel Merck 230–400 mesh and silica gel F254 plates (Merck) respectively. For compound detection the TLC plates were sprayed with a freshly prepared solution of 0.5 mL *p*-anisaldehyde in 50 mL glacial acetic acid and 1.0 mL 97% sulphuric acid and then heat to 105° C until maximum visualization of spots.

FTIR measurements were carried out in a Perkin Elmer GX spectrophotometer provided with a DTGS detector constantly purged with dry air. The spectra were acquired as liquid film using a demountable cell with ZnSe windows in the 4000 to 400 cm^{-1} range. A total of 256 scans were accumulated. The resolution of the equipment employed was 1 cm^{-1}. The Raman spectrum of carquejol in solid state at room temperature was recorded between 3500 and 50 cm^{-1} with a Thermo Scientific, DRX Raman Microscope equipped with a laser (excitation line of 1532 nm, 10 mW of laser power). The Raman spectrum was recorded with 300 scans and a resolution of 4 cm^{-1}.The ECD spectra of the sample in ethanol 96° at a concentration of 0.1–0.3 mg/mL were recorded in a 1 mm path length quartz cuvette using a Jasco J-815 CD spectrometer.

3. Computational details

Initially the four possible (4*R*,5*R*), (4*S*,5*R*), (4*R*,5*S*) and (4*S*,5*S*) stereoisomers of carquejol respectively called C1, C3, C4 and C5, were built with the *GaussView* program [33] and, then, they were optimized by using the hybrid B3LYP and the 6-31G* and 6-311++G** basis sets [14,15] with the Gaussian 09 program [34]. These four carquejol structures are shown in Fig. 1 where C1 and C5 as well as C3 and C4 represent enantiomeric pairs. The natural product C3 was shown to be enantiomerically pure by chiral GC. In an achiral environment, enantiomers present identical physical and chemical properties and differ from one another only by their interaction with polarized light. Consequently, only diastereomers C1 and C3 should be considered as they are energetically identical to C4 and C5 respectively. In order to optimize C1 and C3 structures, the potential energy surfaces (PES) described by the dihedral C6–C5–C11–C19 angles were studied using both levels of theory which for the 6-31G* basis set are presented in Fig. S1. These graphics show only two most stable conformations named C1-1 and C1-2 for (4R,5R) configuration and also two stable conformations named C3-1 and C3-2 for (4S,5R) configuration which are shown in Fig. S2. For those four carquejol conformations, two types of charges were studied: the natural population analysis (NPA) and the Merz-Kollman (MK) charges [35]. Then, and by using the latter charges, the molecular electrostatic potentials were also calculated. The bond orders and the donor-acceptor interactions were computed with the NBO calculations [16] while the topological properties were determined with the AIM2000 program [18]. In this work, the frontier orbitals were calculated in order to predict the reactivities of all structures using their gap values [21–25] and subsequently, with these values the chemical potential (μ), electronegativity (χ), global hardness (η), global softness (S) and global electrophilicity index (ω) descriptors were calculated [26–29] by using both levels of theory. The force fields of those stable configurations of carquejol were calculated with the SQMFF procedure [19] and the Molvib program [20] using normal internal coordinates similar to other terpenic compounds previously reported by our group [26–29]. The vibrational assignments were performed considering the potential energy distribution (PED) contribution ≥ 10% and their IR and Raman spectra. Besides, the ^{1}H and ^{13}C chemical shifts were calculated for all carquejol structures applying both methods and the Gauge-Independent Atomic Orbital (GIAO) method [36] using tetramethylsilane (TMS) as reference. Finally, the ultraviolet–visible spectrum was also predicted in water using Time-dependent DFT calculations (TD-DFT) at the 6-31G* and 6-311++G** levels of theory with the Gaussian 09 program [34]. Moreover, the TDDFT calculations were also employed to predict the rotatory strengths for all conformers in order to find the absolute configuration of carquejol by ECD.

4. Results and discussion

4.1. Structural study

Calculated total and relative energies, dipolar moment and population values for the four most stable conformers of carquejol (Fig. S2) in gas phase by using both methods are shown in Table 1. Values obtained in aqueous and n-hexane solutions are also presented. The theoretical results clearly show that C1-1 is the most stable conformer in all media and, for these reasons, it present the higher populations with both level calculations. It is worth to note that in the absolute configuration (4*S*,5*R*) determined by Snatzke et al. [13] for natural carquejol from *B. trimera*, the isopropenyl and hydroxyl groups possess a *cis* configuration and a conformation corresponding to that indicated as C3-1, while the most stable conformer C1-1 has (4*R*,5*R*) configuration with the hydroxyl and isopropenyl groups on opposite sides (*trans*). Table 1 also shows that both C3 structures present the higher relative energies in gas phase and, consequently, the lower populations in that medium. However, when the dipole moment values for the C1-1, C1-2, C3-1 and C3-2 conformers in gas phase are graphically represented by using the B3LYP/6-31G* method we observed that the magnitude, direction and orientation of their vectors in all these structures were different among them, as shown in Fig. S3. Hence, the dipole moment values observed for C3-1 could probably explain their presence in the solid phase, as reported for other compounds [37–40]. Obviously, these results could have influence on their electronic properties and probably their reactivities and behaviours in the different media.

So far, the experimental geometrical parameters for carquejol were not reported and, for this reason, the theoretical geometrical parameters calculated for the four conformers in the gas phase were compared with structures experimentally determined for other terpenes containing similar groups such as, those structures determined for the diterpene*rac*-(1*R*,2*R*,3*S*,7*S*)-3-hydroxy-5-isopropyl-2-methyltricyclo[8.4.0.$0^{2,7}$]-4,9-tetradecadien-6-one(CembraneDiterpene) by X-ray diffraction by Caracelli et al. [41] and for 7-methyl-16-oxo-4,10-bis(prop-1-en-2-yl)-17,18-dioxa-14,15-diaza-tetra-cyclo-[9.4.2.$1^{6,9}$.$0^{1,12}$]octa-deca-6,8,14-trien-5-yl acetate](KAP) determined by Rodríguez-Escudero et al. [42]. Fig. S4 shows the structures of those two compared compounds indicating with circles the similar groups to carquejol. Table 2 shows the comparisons among the geometrical parameters calculated and experimental by means of root-mean-square deviation (RMSD). In general, we observed a good correlation in the bond lengths for the four structures but a better agreement is observed for C1-1, C1-2 and C3-1 with both basis sets with values between 0.020 and 0.019 Å while for the bond angles a better correlation is principally observed for C-11 and C1-2 (3.0–2.9°). Here, the bond lengths and

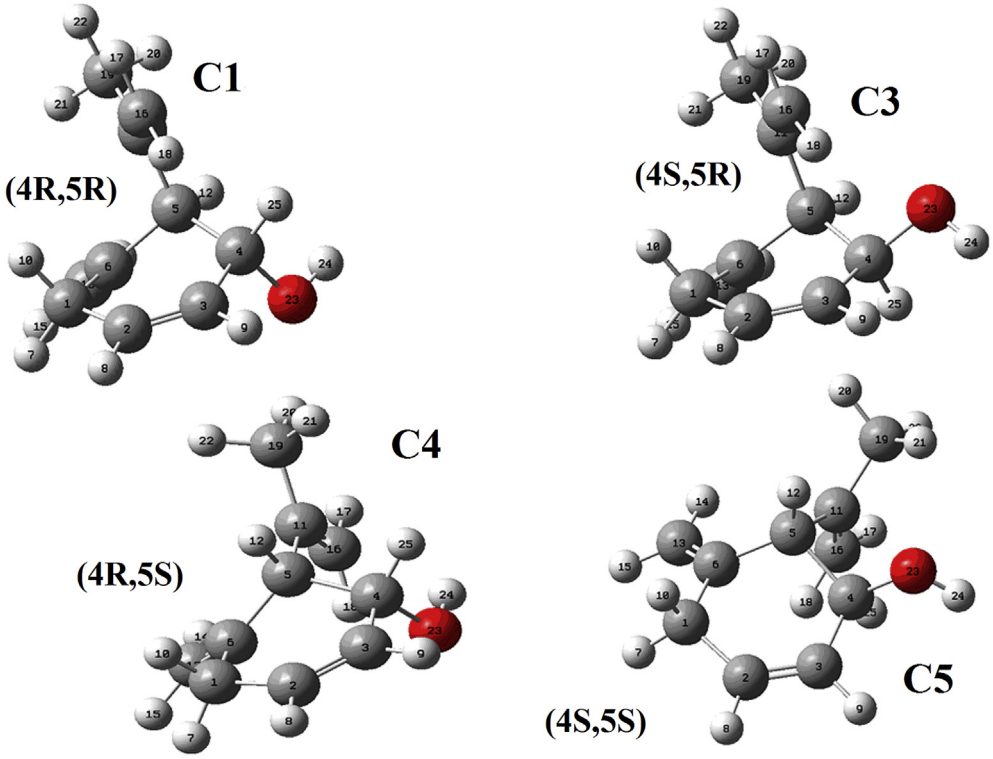

Fig. 1. Molecular structures of the most stable conformers of carquejol and atoms numbering.

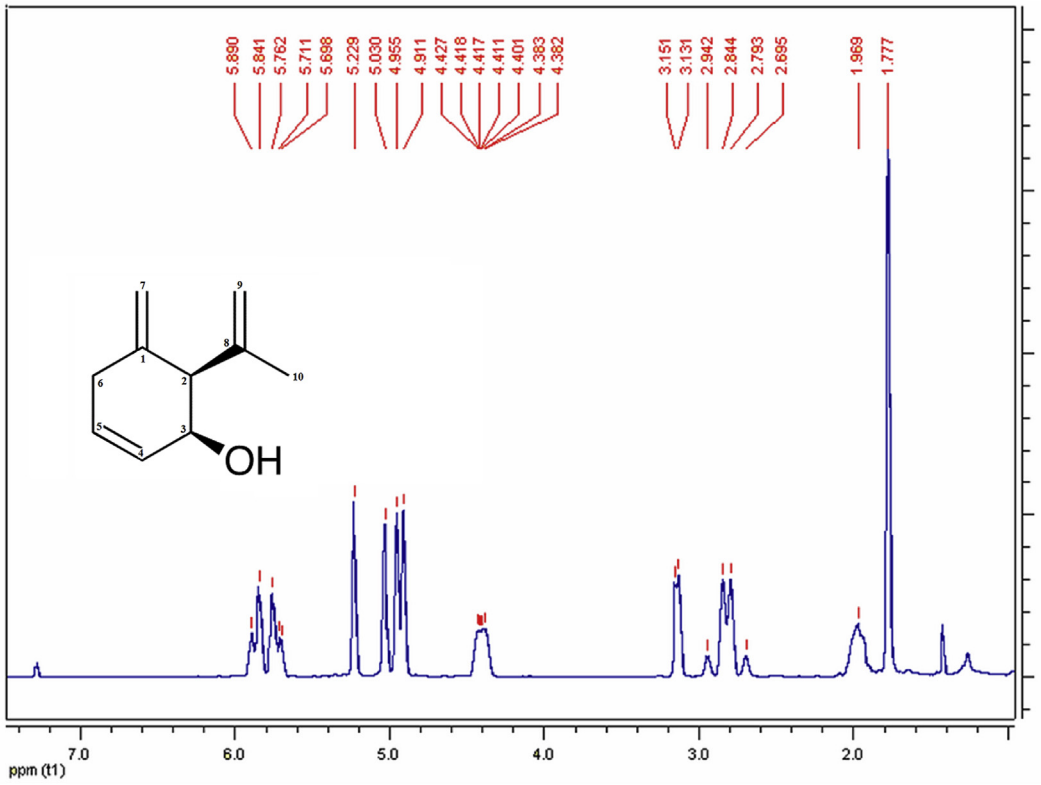

Fig. 2. ^{1}H NMR spectrum of (4*S*,5*R*)-carquejol in $CDCl_3$.

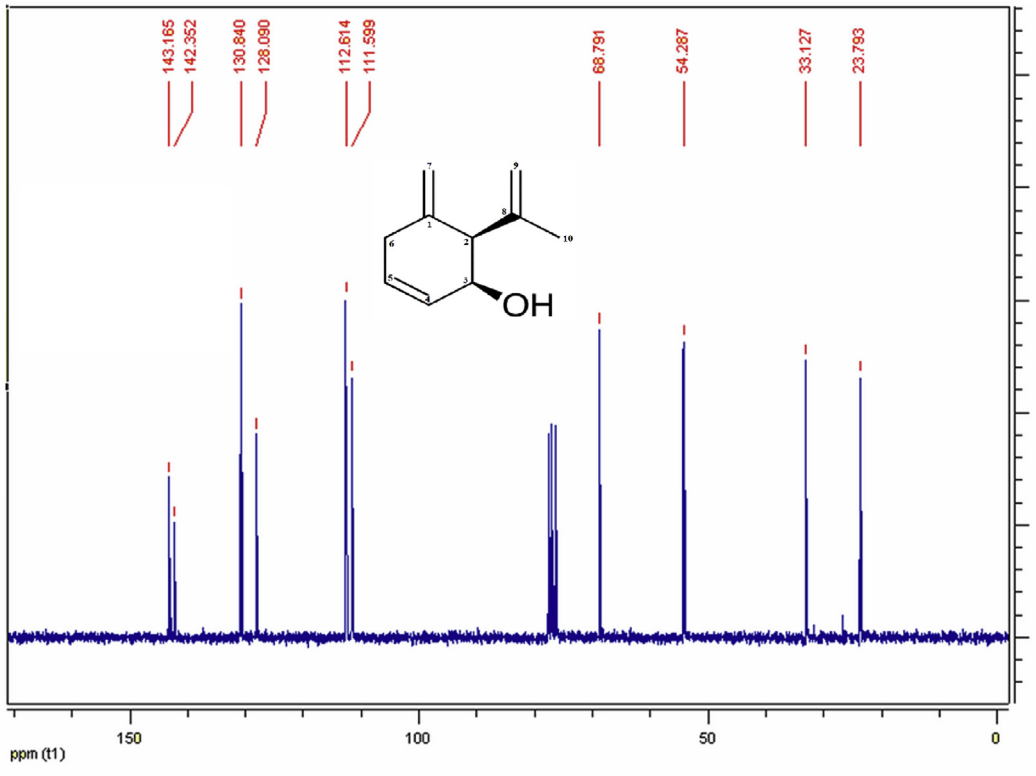

Fig. 3. ^{13}C NMR spectrum of (4*S*,5*R*)-carquejol in $CDCl_3$.

Table 1
Calculated total (*E*) and relative energies (Δ*E*), dipolar moment (μ) and population values for the most stable C1-1 and C1-2 conformers of (4*R*,5*R*)-carquejol, and C3-1 and C3-2 conformers of (4*S*,5*R*)-carquejol in gas phase.

Configurations	Conformers	*E* (Hartrees)	*ΔE* (kJ/mol)	*μ* (Debye)	Population%
B3LYP/6-31G*method/Gas phase					
(4R,5R)	C1-1	−464.6431	0.00	1.39	49.30
(4R,5R)	C1-2	−464.6430	−0.26	1.84	44.44
(4S,5R)	C3-1	−464.6405	−6.82	1.59	3.13
(4S,5R)	C3-2	−464.6395	−6.82	2.00	3.13
PCM/B3LYP/6-31G*method/Aqueous solution					
(4R,5R)	C1-1	−464.6513	0.00	2.08	39.43
(4R,5R)	C1-2	−464.6509	−1.05	2.70	25.63
(4S,5R)	C3-1	−464.6483	−0.34	2.31	34.30
(4S,5R)	C3-2	−464.6474	−10.23	2.87	0.64
B3LYP/6-31G*method/N-hexano					
(4R,5R)	C1-1	−464.6536	0.00	1.56	51.65
(4R,5R)	C1-2	−464.6535	−0.26	2.09	46.49
(4S,5R)	C3-1	−464.6485	−9.97	1.91	0.93
(4S,5R)	C3-2	−464.6498	−9.97	2.26	0.93
B3LYP/6-311++G**method/Gas phase					
(4R,5R)	C1-1	−464.7836	0.00	1.61	49.72
(4R,5R)	C1-2	−464.7834	−0.52	1.88	40.28
(4S,5R)	C3-1	−464.7787	−4.18	1.70	9.20
(4S,5R)	C3-2	−464.7797	−10.23	1.97	0.80

angles could explain why C3-1 is the conformation experimentally observed. On the other hand, C1-1, C1-2 and C3-1 show the major variations in the dihedral angles, while the better correspondence is found for C3-2 where the diverse packing of the structures compared could justify the small differences observed. For instance, in the crystalline KAP structure the molecules are linked by weak C—H···O interactions and by an intra-molecular C—H···O hydrogen bond [42] while in cembrane diterpene the molecules are also connected through a hydrogen bond [41]. Here, taking into account that in the KAP structure due to the OH groups the molecules are linked by inter and intra-molecular H bonds, in the structure of carquejol could be expected interactions by H bonds due to the presence of OH bonds in their structure.

4.2. MEP, bond orders, NPA and MK charges

Many authors have reported that the biological properties displayed by sesquiterpenic compounds can probably be related to the structural requirements associated to hydrophobic and hydrophilic sites of these species [43–46] and, for these reasons, the

Table 2
Comparison of calculated geometrical parameters for carquejol compared with those experimental to other terpenes.

B3LYP Method[a]									Exp,[b,c]
Parameter	C1-1		C1-2		C3-1		C3-2		
	6-31G*	6-311++G**	6-31G*	6-311++G**	6-31G*	6-311++G**	6-31G*	6-311++G**	
Bond lengths (Å)									
C4–O23	1.434	1.439	1.431	1.435	1.429	1.432	1.430	1.434	1.428[b]
C1–C2	1.509	1.332	1.507	1.504	1.510	1.504	1.508	1.506	1.508[b]
C2–C3	1.335	1.332	1.333	1.331	1.334	1.331	1.334	1.331	1.334[b]
C3–C4	1.506	1.503	1.509	1.507	1.514	1.508	1.512	1.510	1.490[b]
C4–C5	1.554	1.553	1.545	1.544	1.546	1.551	1.549	1.548	1.550[b]
C5–C6	1.521	1.520	1.527	1.526	1.526	1.522	1.526	1.525	
C6–C13	1.334	1.332	1.334	1.332	1.335	1.333	1.335	1.333	
C5–C11	1.530	1.530	1.523	1.522	1.531	1.534	1.535	1.533	1.524[c]
C11–C19	1.510	1.508	1.510	1.509	1.512	1.508	1.509	1.508	1.524[c]
C11–C16	1.337	1.335	1.336	1.333	1.335	1.334	1.337	1.335	1.385[c]
RMSD	**0.019**	**0.065**	**0.019**	**0.020**	**0.020**	**0.020**	**0.020**	**0.020**	
Bond angles (°)									
C3–C4–O23	106.3	106.5	111.4	111.2	112.4	112.3	112.2	112.1	107.8[b]
C5–C4–O23	111.2	111.2	106.6	106.5	109.2	108.3	108.1	108.2	112.6[b]
C1–C2–C3	123.5	123.5	122.9	122.9	122.8	123.2	123.0	123.0	118.2[b]
C2–C3–C4	123.5	123.5	123.5	123.6	123.4	123.2	123.7	123.7	125.5[b]
C3–C4–C5	113.2	113.5	111.7	112.0	112.4	112.2	112.8	113.1	114.8[b]
C4–C5–C6	110.1	110.2	108.9	109.2	107.1	108.3	108.2	108.2	108.1[b]
C5–C6–C1	114.5	114.5	114.4	114.2	114.8	117.6	116.8	116.9	111.9[b]
C5–C6–C13	122.6	122.6	124.2	124.4	122.5	120.9	121.3	121.3	
C1–C6–C13	122.7	122.7	121.2	121.2	122.6	121.3	121.6	121.6	
C5–C11–C16	124.0	124.0	120.1	120.1	125.1	125.0	118.4	118.4	119.3[c]
C5–C11–C19	114.5	114.5	118.4	118.5	113.6	113.9	120.8	120.8	118.3[c]
C16–C11–C19	121.3	121.3	121.3	121.3	121.1	120.9	120.6	120.7	122.2[c]
RMSD	**2.9**	**2.9**	**3.0**	**3.0**	**3.6**	**4.0**	**3.2**	**3.2**	
Dihedral angles (°)									
C2–C3–C4–O23	−109.1	−111.2	−141.0	−139.0	145.2	148.8	143.9	144.2	146.1[b]
C6–C5–C4–O23	79.8	81.9	170.3	168.5	−173.3	−172.9	−169.9	−169.6	−166.2[b]
C6–C5–C11–C16	101.7	101.5	−96.3	−98.1	107.0	43.1	−98.9	−101.5	−92.5[c]
C6–C5–C11–C19	−77.6	−77.9	83.8	82.3	−72.5	−137.0	81.1	78.7	86.2[c]
C2–C1–C6–C13	135.8	134.9	−145.4	−144.2	136.4	148.2	141.0	141.6	
C4–C5–C6–C13	−122.3	−122.5	124.3	124.8	−117.9	−125.6	−122.3	−123.3	
RMSD	**218.1**	**219.3**	**221.2**	**219.9**	**127.5**	**130.6**	**4.6**	**6.2**	

[a] This work.
[b] Ref [41].
[c] Ref [42].

identifications of these possible reaction sites are of interest in a terpene derivative as carquejol due to their potential pharmacological properties reported [31,32]. In this work, the molecular electrostatic potential (MEP) values for all atoms were calculated from the atomic Merz-Kollman (MK) charges [35] while the MEP mapped surfaces for C1-1, C1-2, C3-1 and C3-2 structures were built using the *GaussView* program [33]. The forces of the different bonds are also related to those reactivity sites because when a bond is weak, the break of that bond is expected, so, for this reason, the bond order (BO) values is other very important property. Thus, for all structures of carquejol in gas phase, the MEP and BO expressed as Wiberg indexes are summarized respectively in Table S1 and S2 by using both levels of theory. Analyzing, the MEP values we observed the following tendency: O > C > H, as expected due to the electronegativity values of the O atoms but, for the C atoms we observed the higher values on the C13 and C16 atoms, both belonging to the $=CH_2$ groups, while the lower values are observed on the C4 atoms linked to the O23 atoms belonging to the OH groups. In relation to the values for the H atoms, the less negative values are observed on the H24 atoms, as expected because these atoms are linked to the O23 atoms and, as a consequence they are the most labile. Regarding the mapped MEP surfaces of the C1-1, C1-2, C3-1 and C3-2 conformers, which are presented in Fig. S5, we observed the typical red and blue colorations of those nucleophilic and electrophilic sites, respectively. This way, these two reaction sites are clearly defined on the OH groups. Practically, there are not significant differences observed among those surfaces. In relation to the BO values, Table S2 show that the C6 and C11 atoms have the higher values because they are linked to C=C groups and, for this reason, both atoms have higher sp^2 character while the C4 and C19 present the lower BO values because in the C11–C19 bond the C19 atom has 71.31% p character versus the C11 which has 69.19%. On the contrary, in the C4–O23 bond the C4 atom has a 79.82% of p character while the O23 atom only the 69.64%, hence, those BO values are clearly justified. As expected, the H24 atoms are the most labile and, as a consequence, they present the lowest BO values. In general, when increase the size of the basis set the BO values increase but in the MEP values there are no observed a defined tendency because some (C and O atoms) values increase while other decrease their values (H atoms). Here, probably the higher MEP observed on the C11, C13 and C16 atoms of all conformers could probably explain the directions and orientations observed in their dipole moments.

The charges are other important property deeply related to the MEP values and to the charges distribution in a molecule. In particular, we need to explain why the dipole moment values have different directions and orientations. For these reasons, the atomic natural population (NPA) and Merz-Kollman (MK) charges were studied for all conformers of carquejol. The calculated MK and NPA results in gas phase and with both levels of theory are observed in Tables S3 and S4, respectively. First, we observed that both charges are different between them and, in particular, the NPA charges on

all the atoms are higher than the other ones. Second, the MK charges observed on the C4, C5, C11, C13 and C16 atoms present slightly variations in all conformers with both basis sets, as shown in Fig. S6. The graphics clearly show that the behaviour of the MK charges on the C4 and C11 atoms are different in all conformers by using both basis sets. On the contrary, the NPA charges on those atoms practically do not present modifications in all conformers. This way, the orientations and directions of the dipole moment value observed could be easily explained by the MK charges.

4.3. Stability studies

All species of carquejol were also studied by NBO [16] and AIM [17,18] calculations in order to examine their stabilities because some components of *B. trimera* shows strong anti-inflammatory and analgesic properties probably due to the inhibition of prostaglandins production [3]. Here, these studies were performed for all those forms considering the donor-acceptor energy interactions and their topological properties in gas phase. The donor-acceptor energy interactions computed for all conformations by using the two levels of theory are presented in Table S5 while the topological properties are shown from Tables S6 to S8. The NBO results for all structures showed three different types of interactions: $\Delta ET_{\pi\rightarrow\sigma^*}$, $\Delta ET_{\sigma\rightarrow\sigma^*}$ and $\Delta ET_{LP\rightarrow\sigma^*}$ which are related to the double bonds of the cyclohexene ring (C═C), to the ═CH_2 groups of the side chain and, to the lone pairs of the O23 atoms, where clearly we observed that the energy of the interactions are completely different with both basis sets. Thus, one $\pi(2)C2-C3 \rightarrow \sigma^*C4-O23$, four $\sigma C-H \rightarrow \sigma^*C-C$ and the $LP(2)O23 \rightarrow \sigma^*C-C$ interactions were observed in all the conformers. Hence, C1 is the most stable stereoisomer of carquejol because it has the higher total energy ΔE_{Total} with both basis sets while this same value of energy is also observed for C3-2 by using the other basis set. In consequence, the influence of the size basis set is clearly observed in this study and, for these reasons, the presence of both C3-1 and C3-2 conformations can be expected in solid phase, as evidenced experimentally [13].

The stabilities of those structures of carquejol were also studied through their topological properties with the AIM program [18]. In this study, the possible intra-molecular interactions were determined with Bader's theory [17] calculating the topological properties such as, the electron density distribution, $\rho(r)$ in the bond critical points (BCPs), the values of the Laplacian, $\nabla^2\rho(r)$, the eigenvalues $(\lambda1, \lambda2, \lambda3)$ of the Hessian matrix and the $\lambda1/\lambda3$ ratio. These parameters are important to identify the characteristics and type of interaction, hence, in Table S6 is given those parameters for C1-1 and C1-2 while in Tables S7 and S8 are summarized the parameters for C3-1 and C3-2, respectively, computed for both levels of theory in the bond critical points (BCPs) and ring critical points (RCPs). Notice that when an interaction present high values of $\rho(r)$ and $\nabla^2\rho(r)$, the ratio $\lambda1/\lambda3 > 1$ and $\nabla^2\rho(r) < 0$ the interaction is covalent (shared interaction) and, on the contrary, the interaction is ionic or highly polar covalent when $\lambda1/\lambda3 < 1$ and $\nabla^2\rho(r) > 0$ (closed-shell interaction). Regarding deeply Table S6 we observed only one H bond interaction for C1-1 using the 6-31G* basis set while in C1-2, there are not observed H bonds interactions but, the presence of two H bonds in C3-1 and of three H bonds in C3-2 with both basis sets could clearly justify their experimental presence in the solid phase. In these latter forms, RCP1and RCP2 are the new ring critical points while RCP3 is the RCP belong to the cyclohexene ring. Fig. S7 shows details of the molecular model for the C1-1 conformer of carquejol. On the contrary, for C1-2 with both basis sets are predicted only the RCP corresponding to the cyclohexene ring. These studies obviously support the high stabilities of both C3 conformers, especially of C3-2 due to the presence of three different O–H, H–H and C–C interactions.

4.4. Frontier orbitals and descriptors

The calculations of the gap energy values by using the frontier orbitals are properties interesting to predict the reactivities and behaviours of different species in all the possible media, as initially was reported by Parr and Pearson [21]. In particular, the evaluations of the chemical potential (μ), electronegativity (χ), global hardness (η), global softness (S) and global electrophilicity index (ω) descriptors by using the gap values are useful to estimate the behaviours of those conformers in relation to their potential pharmacological activities [6,31,32]. Thus, the gap values for all species together with those descriptors were calculated using both levels of theory. These results are shown in Table S9 together with the thiol and thione forms of 1,3-benzothiazole tautomers a compound with potential antimicrobial activity [24] and with cidofovir and brincidofovir [29], two antiviral drugs against to *Ebola* virus disease. By comparing first the gap values for all conformers, we observed that the values for the conformers were strongly dependent of the size of the basis set, thus, C1-1 was the most reactive using the 6-31G* basis set but by using the 6-311++G** basis set C1-2 exhibited the higher reactivity. On the other hand, the C3-1 and C3-2 forms were the most reactive with both basis sets. When the gap values were compared with the values for the thiol and thione [24] forms and with the antiviral cidofovir and brincidofovir [29], carquejol clearly was much less reactive than those four species. For a better comparison the structures of these compounds are presented in Fig. S8. The presence of NO_2 groups in the 1,3-benzothiazole tautomers and, of PO_4 groups in those antiviral compounds, clearly increase their reactivities. When the gap values for those structures of carquejol were compared with the corresponding values for other terpenoids, such as cnicin (−4.8217 eV) [27] and onopordopicrin (−5.0523 eV) [47] we observed that the presence of a higher number of C═O and C═C double bonds, of OH groups and of O atoms increased the reactivities of these compounds and, for these reasons, decreased significantly their gap values when they were compared with the carquejol conformers. In relation to the descriptors, the hardness and softness are related to the lower and higher reactivity, respectively, thus, obviously, for carquejol are expected higher hardness and lower softness than those compounds with antimicrobial and antiviral activities. The global electrophilicity index is also lower in carquejol while the global nucleophilicity index is higher in carquejol with both basis sets. When the ω and E values are compared with those determined for cnicin of 3.54 and −9.96 eV, respectively [27] and for onopordopicrin of 3.35 and −10.36 eV, respectively [47] the values are comparable with carquejol only for E (−9.91 eV in C3-1 and −10.34 eV in C5 using 6-31G* basis set). This way, the pharmacological properties observed in carquejol could be easily justified by the nucleophilicity index because the two values are similar to those observed for onopordopicrin and cnicin which show several biological activities too.

4.5. NMR study

The experimental ^1H and ^{13}C NMR spectra of carquejol in $CDCl_3$ are shown in Figs. 2 and 3, respectively while the 2D $^1H-^1H$ gCOSY, $^1H-^{13}C$ gHSQC, $^1H-^{13}C$ gHMBC spectra are given in Figs. S9a, S10 and S11, respectively. The expansions of the ^1H NMR spectrum are presented as supporting material in Fig. S9b and S9c. Here, the 2D spectra were used for multiplicity determinations and are very important because they show the spin-spin coupling between the hydrogen atoms of the molecule (gCOSY experiment), hydrogen atoms directly bonded to carbon (HSQC experiment) and long distance (two and three bonds) correlation of C with H

(HMBC experiment). The predicted ^{1}H and ^{13}C NMR chemical shifts for the most stable configurations of carquejol calculated by using the GIAO method [36] and with both basis sets are compared with the corresponding experimental ones in Tables S10 and S11, respectively by using the RMSD values. In general, the theoretical values are overestimated in relation to the experimental ones and a better concordance for the ^{1}H nucleus (0.4–0.2 ppm) of all conformers than for the ^{13}C nucleus (24.7–8.1 ppm) was observed. As expected, the better correlations were obtained for all conformers with the 6-311++G** basis set because this basis set generate better-quality results for the ^{1}H nucleus than the C atoms and than the 6-31G* basis set. Here, the similarity in the RMSD values for both H and C nucleuses, for C3-1 and C3-2 by using the two basis sets, could probably suggest the presence of these structures in the liquid phase and probably also will be present in the solid state.

4.6. Vibrational study

Fig. 4 shows the experimental IR and Raman spectra of carquejol in the solid phase while Figs. 5 and 6 can be seen the comparisons between the predicted IR and Raman spectra for C3-1 and C3-2 in gas phase with the corresponding experimental ones because the (4S,5R) conformation, corresponding to C3-1, was experimentally observed in the solid phase. Fig. 5 shows a reasonable concordance between the two intense bands located in approximately 1000 cm^{-1} region in the IR spectrum of C3-2 with the corresponding experimental one. Here, the predicted Raman spectra were expressed in relative Raman intensities after the conversion from scattering activities by using equations reported by other authors [48,49]. On the other hand, in Figs. S12 and S13 can be seen the predicted infrared and Raman for all conformations in gas phase. All structures of carquejol were predicted with C_1 symmetries and, for this reason, 69 vibration normal modes are expected for these species and, where all the modes present activities in both spectra. The complete assignments were performed using the SQMFF methodology [19] and the Molvib program [20]. The internal coordinates for those structures were similar to the reported for other terpenes [26–28,47]. Here, the force fields were computed with both basis sets but the assignments were performed by using the B3LYP/6-31G* level of theory because the scale factors are reported for this level of theory [19]. Table 3 shows the observed and calculated wavenumbers and assignments for the most stable

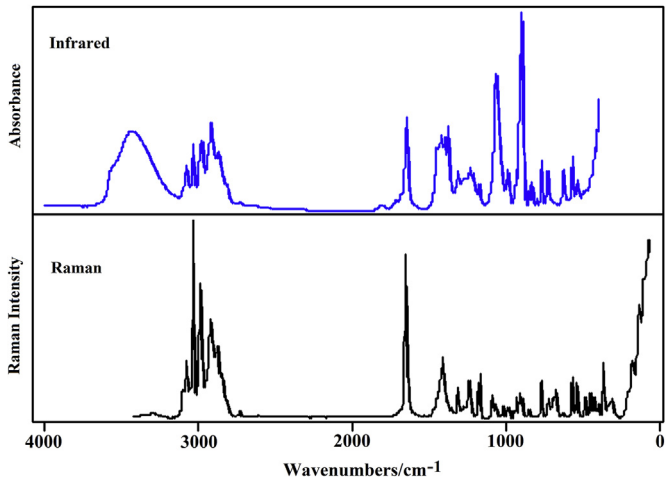

Fig. 4. Experimental infrared (upper) and Raman spectra (bottom) of (4*S*,5*R*)-carquejol in the solid state.

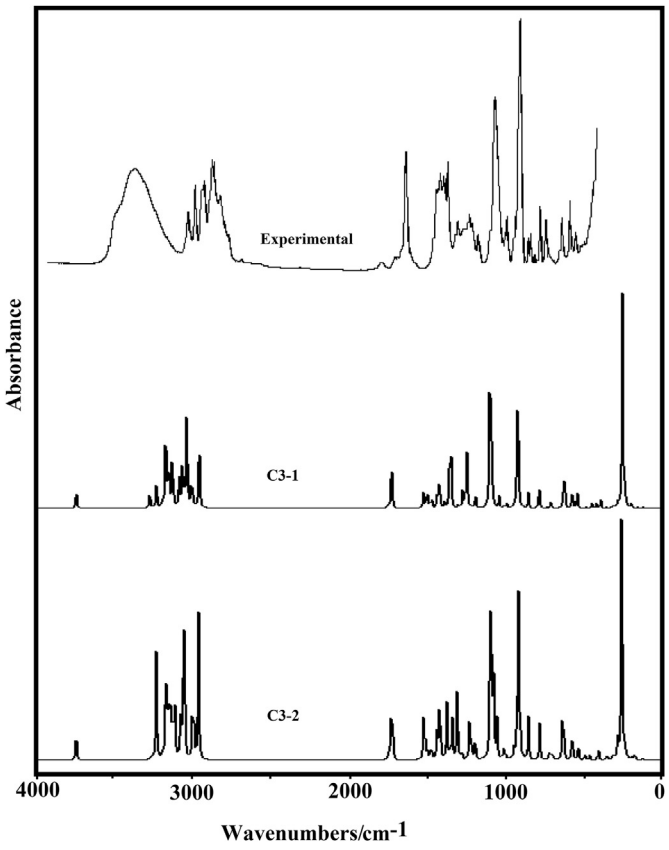

Fig. 5. Experimental infrared in the solid state of (4*S*,5*R*)-carquejol compared with the corresponding predicted for C3-1 and C3-2 conformers by using B3LYP/6-31G* level of theory.

configurations of carquejol using the B3LYP/6-31G* level of theory and those potential energy distribution (PED) contributions $\geq$ 10%. Fig. S12 shows clear differences between the predicted infrared spectra where the intensities and forms of the observed bands in the 1000 cm^{-1} region probably justify the presence of C3-1. Here, the group of bands in the Raman spectra (Fig. S13) between 800 and 700 cm^{-1} probably support the presence of C3-1 and C3-2 in the solid state because they show the same features than the experimental ones. A brief discussion on the assignments of some groups follows.

4.6.1. Band assignments

4.6.1.1. OH modes. Usually, in compounds containing OH groups such as thymidine or some terpenes, the OH stretching modes are assigned between 3480 and 3254 cm^{-1} [22,27–29], hence, the very strong IR band at 3431 cm^{-1} is without difficulty assigned to that vibration mode, as observed in Table 3. Structurally, we expected intermolecular interactions for the conformations of carquejol because in the higher wavenumbers region Fig. 5 shows clearly the typical broad band associated to inter-molecular O–H bonds, as was reported for thymidine by Görbitz et al. [50]. The in-plane deformation or rocking modes are assigned to the IR and Raman bands between 1204 and 1166 cm^{-1} because they are predicted by calculations in this region. Note that for C1-1 and C3-1 these modes are predicted as pure mode but for C1-2 and C3-2 these modes are coupled with other modes. The SQM calculations predicted the out-of-plane deformation modes between 269 and 228 cm^{-1}, hence; these modes are assigned to the shoulders and Raman band at 295, 241 and 218 cm^{-1}, as indicated in Table 3.

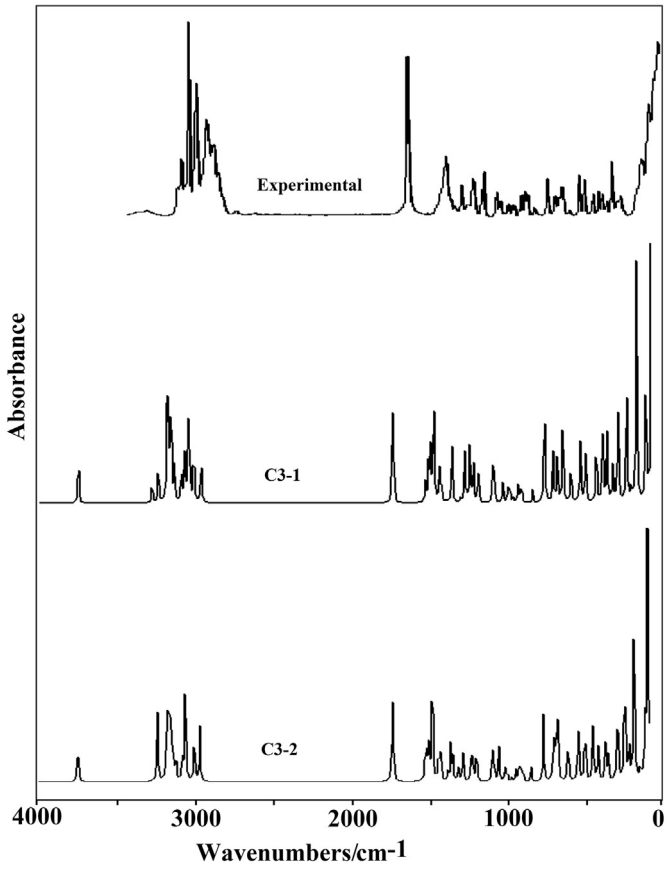

Fig. 6. Experimental Raman in the solid state of carquejol compared with the corresponding predicted for C3-1 and C3-2 conformers by using B3LYP/6-31G* level of theory.

4.6.1.2. CH modes. In the conformers of carquejol there are two C–H stretching modes (C2–H8 and C3–H9 bonds) where the C atoms have sp^2 hybridization while other two have sp^3 hybridization (C4–H25 and C5–H12 bonds), later, all these modes are predicted in different regions. This way, the C2–H8 and C3–H9 stretching modes are predicted by the SQM calculations between 3054 and 3012 cm^{-1} and, for this reason, the shoulders and bands observed between 3075 and 3021 cm^{-1} are assigned to these modes, as expressed in Table 3. The C2–H8 and C3–H9 rocking modes for all conformers are predicted between 1377 and 1157 cm^{-1}, hence, they are assigned in these regions, as summarized in Table 3. It is necessary to clarify that the CH rocking modes corresponding to the C atoms with sp^2 hybridization are identified by the β symbol while the other ones by the ρ symbol, as reported for compounds with rings [22–24,26–30]. Obviously, the out-of-phase modes are expected only for those two C2–H8 and C3–H9 bonds with sp^2 hybridization, which for all conformers are assigned to the IR bands at 997, 985, 768, 726 and 700 cm^{-1}, in accordance with the calculations.

4.6.1.3. CH_3 modes. Carquejol conformers have only a CH_3 group, hence only three stretching modes are expected and, where all SQM calculations predicted these modes as fully pure in different regions. The shoulders and the IR bands at 3021, 2978, 2971 and 2915 cm^{-1} are assigned to the antisymmetric and symmetric stretching modes, as detailed in Table 3. Here, the symmetrical modes are clearly assigned to a strong Raman bands. The CH_3 deformation modes are assigned between 1587 and 1436 cm^{-1} in accordance with the calculations while the rocking and twisting modes are predicted in the 1084/1026 and 220/171 cm^{-1} regions and, therefore, they were assigned as predicted by SQM calculations and, as can be seen in Table 3.

4.6.1.4. CH_2 modes. For all conformers of carquejol, there are three types of CH_2 groups, two with sp^2 hybridization (=CH_2) where the H atoms are linked to the C13 and C16 atoms and, a group with sp^3 hybridization where the H atoms are linked to the C1 atoms. Obviously, the =CH_2 stretching modes are predicted at higher wavenumbers than the other ones and, for these reasons, they are assigned in accordance with the calculations. Note that the very strong Raman band at 3032 cm^{-1} is easily assigned to the symmetrical modes corresponding to the two =CH_2 groups. The antisymmetrical and symmetrical modes for the other CH_2 group are assigned in the same region but at lower wavenumbers, as indicated in Table 3. The SQM calculations predicted the CH_2 deformation, rocking, waging and twisting modes for the two conformers at higher wavenumbers than the other two =CH_2 groups. Hence, they were assigned accordingly to the B3LYP/6-31G* calculations and, as shown in Table 3.

4.6.1.5. Skeletal modes. The C–O stretching modes in all conformers of carquejol are predicted between 1063 and 1020 cm^{-1}, thus, the very strong IR band at 1065 cm^{-1} and the shoulder associated to that intense band are assigned to the stretching modes of all conformers. The C2=C3, C11=C16 and C6=C13 stretching modes are predicted by the SQM/B3LYP/6-31G* calculations between 1680 and 1659 cm^{-1}, as observed in similar terpenes [27,28,47]; hence, they are clearly assigned in that region. On the other hand, the C–C stretching modes were assigned between 1303 and 652 cm^{-1}, as predicted by the SQM calculations and, as observed in Table 3. The deformation and torsion ring modes are predicted in approximately the same regions reported for other terpenes [27,28,47] and, as a consequence they are clearly assigned in those regions. Table 3 shows the assignments of the remaining skeletal modes expected for all conformers of carquejol.

5. Force fields

The force constants for all conformers of carquejol were computed in gas phase with the SQMFF procedure [19] and the Molvib program [20] using their corresponding scaled force fields at the B3LYP/6-31G* and 6-311++G** levels of theory. They were compared with those reported for cnicin [27], 13-*epi*-sclareol [28] and onopordopicrin terpenes [47] in Table 4. Comparing first the force constants for all conformers of carquejol, we observed an slight increase in the $f(\nu O–H)$, $f(\nu CH_2)$, $f(\nu C–O)_c$ force constants values using the 6-31G* basis set of C1-2, C3-1 and C3-2, in relation to those observed for C1-1, while only a decrease in the $f(\nu C–H)$ force constant of those three forms are observed with the same basis set. Here, the higher values observed for $f(\nu{=}CH_2)$ in reference to $f(\nu CH_2)$ are in agreement with the higher wavenumbers observed for those groups where the C atoms have sp^2 hybridization. Note that the $f(\delta{=}CH_2)$, $f(\delta CH_2)$ and $f(\delta C–OH)$force constants do not change their values when the size of the basis set increase to 6-311++G**. These similarities in those force constants can be clearly attributed to the proximities observed in the geometrical parameters of all conformers, as observed in Table 2. When the values for all species of carquejol are compared with those corresponding to the other three terpenic compounds small differences were observed among their values. These differences are obviously related to the different number of OH, C=O, C=C groups, of O atoms and, to the nature of these groups present in their structures. Thus, the presence of C=C and OH groups in carquejol, analogous

Table 3
Observed and calculated wavenumbers (cm^{-1}) and assignments for the most stable conformers of (4*R*,5*R*)-carquejol and (4*S*,5*R*)-carquejol.

Experimental[a]		C1-1[a]		C1-2[a]		C3-1[a]		C3-2[a]	
IR	Ra	SQM[b]	Assignments[a]	SQM[b]	Assignments[a]	SQM[b]	Assignments[a]	SQM[b]	Assignments[a]
3531sh	3357vw	3571	νO23–H24	3584	νO23–H24	3585	νO23–H24	3585	νO23–H24
3431vs									
	3291vw	3111	ν_aCH_2(C16)	3112	ν_aCH_2(C13)	3133	ν_aCH_2(C16)		
	3100w			3098	ν_aCH_2(C16)			3098	ν_aCH_2(C16)
	3100w	3096	ν_aCH_2(C13)			3095	ν_aCH_2(C13)	3097	ν_aCH_2(C13)
3075 m	3076w	3054	νC3–H9	3041	νC2–H8	3042	νC2–H8	3040	νC2–H8
3032s	3032vs	3034	ν_sCH_2(C16)	3033	ν_sCH_2(C13)	3035	ν_sCH_2(C16)		
3032s	3032vs	3029	νC2–H8					3026	ν_sCH_2(C16)
3032s	3032vs	3024	ν_sCH_2(C13)	3025	ν_sCH_2(C16)	3023	ν_sCH_2(C13)	3024	ν_sCH_2(C13)
3021sh	3021sh			3014	νC3–H9	3015	νC3–H9	3012	νC3–H9
3021sh	3021sh	2999	ν_aCH_3	2995	ν_aCH_3	2997	ν_aCH_3	3002	ν_aCH_3
2978sh	2982s							2985	ν_aCH_3
2971s	2970sh	2957	ν_aCH_3	2966	ν_aCH_3	2955	ν_aCH_3	2947	νC5–H12
2933sh	2937sh	2942	ν_aCH_2(C1)	2926	ν_aCH_2(C1)	2935	ν_aCH_2(C1)		
2915vs	2918s	2907	ν_sCH_3	2916	ν_sCH_3	2913	νC5–H12	2930	ν_sCH_3
2915vs	2918s	2893	νC5–H12	2896	νC5–H12	2905	ν_sCH_3	2926	ν_aCH_2(C1)
2864 m	2873 m	2876	ν_sCH_2(C1)	2862	ν_sCH_2(C1)	2880	ν_sCH_2(C1)	2872	ν_sCH_2(C1)
	2841w	2869	νC4–H25	2857	νC4–H25				
2810w	2823w					2833	νC4–H25	2838	νC4–H25
2727vw	2725vw		1422 + 1310 = 2732						
1805w									
1715w									
1644s	1653vs	1677	νC2=C3	1680	νC2=C3	1674	νC11=C16	1675	νC2=C3
1644s	1653vs	1670	νC6=C13	1669	νC11=C16	1672	νC2–C3	1665	νC6=C13
1644s	1653vs	1662	νC11=C16	1667	νC6=C13	1663	νC6=C13	1659	νC11=C16
1587vw		1524	δ_aCH_3	1528	δ_aCH_3	1524	δ_aCH_3	1523	δ_aCH_3
1516vvw		1508	δ_aCH_3	1514	δ_aCH_3	1509	δ_aCH_3	1513	δ_aCH_3
1450 m	1460sh	1492	δCH$_2$(C1)	1492	δCH$_2$(C1)	1491	δCH$_2$(C1)	1496	δCH$_2$(C1)
1436 m	1434sh	1441	δ_sCH_3	1439	δ_sCH_3	1442	δ_sCH_3	1442	δ_sCH_3
1422vs		1427	δCH$_2$(C13)					1422	δCH$_2$(C13)
1422vs	1410 m	1416	ρC4–H25	1416	δCH$_2$(C13)	1419	δCH$_2$(C13)		
1402sh		1409	δCH$_2$(C16)	1414	δCH$_2$(C16)	1412	δCH$_2$(C16)	1414	δCH$_2$(C16)
1393vs				1396	βC3–H9	1395	βC2–H8	1396	βC3–H9
									βC2–H8
1374vs	1377sh	1377	βC3–H9	1380	ρ′C4–H25	1385	ρ′C4–H25	1379	ρ′C4–H25
1354sh	1355vw	1350	ρ′C4–H25	1349	ρC4–H25	1354	ρC5–H12	1346	wagCH$_2$(C1)
	1339vw	1342	wagCH$_2$(C1)	1342	wagCH$_2$(C1)	1341	wagCH$_2$(C1)	1339	ρC4–H25
1310 m	1312w	1309	ρ′C5–H12			1319	ρC4–H25	1309	ρ′C5–H12
1303sh	1300vw			1300	ρ′C5–H12,νC5–C6				
1274sh	1275vw	1281	ρC5–H12	1281	ρC5–H12,			1276	ρC5–H12
					νC5–C11				ρCH$_2$(C13)
1263sh	1264vw	1254	ρ′C5–H12, ρCH$_2$(C1)	1273	ρC5–H12	1274	βC6–C13	1271	νC5–C11
1248vw				1248	ρCH$_2$(C1)	1247	ρ′C5–H12	1250	ρC5–H12
					ρCH$_2$(C13)				
1232 m	1238w	1223	ρCH$_2$(C16)			1232	ρCH$_2$(C16)		
							νC19–C11		
	1229sh	1220	ρCH$_2$(C1)						
1216w						1215	ρCH$_2$(C1)	1212	ρCH$_2$(C1)
1204sh				1206	ρCH$_2$(C1), βC3–H9	1202	δO–H		
1171w	1184w	1197	δO–H	1181	ρ′C4–H25, ρC5–H12			1190	ρ′C4–H25, δO–H
1166sh	1169 m	1157	βC2–H8	1165	βC2–H8,	1162	βC3–H9	1162	δO–H
					δO–H				
1090sh	1090w	1080	ρ′CH$_3$	1083	ρ′CH$_3$	1081	ρ′CH$_3$	1084	ρ′CH$_3$
1065vs	1065w	1068	ρCH$_3$, νC4–C5			1067	νC4–C5	1059	νC4–O23
1065vs	1065w	1034	νC4–O23, ρCH$_3$	1063	νC4–O23	1063	νC4–O23	1052	νC4–C5
1042sh	1042vw	1020	νC4–O23	1045	ρCH$_3$			1045	ρCH$_3$
1031sh				1030	νC4–C5	1026	ρCH$_3$		
1002sh	1016vw			1003	νC5–C11				
997w	997sh	994	γC2–H8					990	γC2–H8,γC3–H9
985 m	987vw	987	ρCH$_2$(C13)	988	γC2–H8	986	γC2–H8	987	ρCH$_2$(C13)
985 m	987vw	976	νC5–C11	982	ρCH$_2$(C16)	982	ρCH$_2$(C13)	978	ρCH$_2$(C16)
976sh		958	τwCH$_2$(C1)	949	νC3–C4	963	νC5–C11,νC5–C6		
934 m	937sh			945	τwCH$_2$(C1), νC1–C2	949	τwCH$_2$(C1)	948	τwCH$_2$(C1)
934 m	931w	926	βR$_1$			919	wagCH$_2$(C13)	924	βR$_1$,νC5–C6
918sh	918sh	917	wagCH$_2$(C16)	918	wagCH$_2$(C13)	915	wagCH$_2$(C16)	914	wagCH$_2$(C13)
910sh	911w			913	wagCH$_2$(C16)	912	wagCH$_2$(C16) νC1–C2	908	wagCH$_2$(C16)
910sh	911w	907	wagCH$_2$(C13)	908	wagCH$_2$(C13), τwCH$_2$(C1)	907	wagCH$_2$(C13)	903	νC1–C2
897vs	896w	898	νC1–C2	881	νC19–C11	898	νC1–C2,βR$_1$	884	νC19–C11
897vs	896w	867	δ_C11C5C4						
846w	850w	861	νC3–C4,νC19–C11						
829 m	830vw			839	δ_C11C5C6, νC1–C6	828	νC1–C6	825	νC1–C6
800w									
768 m	770 m	769	νC1–C6	747	βR$_1$, νC1–C6	755	γC3–H9	747	γC3–H9,νC5–C11

(*continued on next page*)

Table 3 (*continued*)

Experimental[a]		C1-1[a]		C1-2[a]		C3-1[a]		C3-2[a]	
IR	Ra	SQM[b]	Assignments[a]	SQM[b]	Assignments[a]	SQM[b]	Assignments[a]	SQM[b]	Assignments[a]
726 m	722w	717	γC3–H9						
700w	695w			705	γC3–H9	695	νC3–C4	692	νC3–C4
675w	676w	666	τwCH$_2$(C13)						
		652	τwCH$_2$(C16),νC5–C6	652	τwCH$_2$(C16)	659	τwCH$_2$(C13)	656	τwCH$_2$(C16)
				643	τwCH$_2$(C13)			642	τwCH$_2$(C13)
626 m	631w					629	τwCH$_2$(C16)	623	γC2–H8
									τwCH$_2$(C16)
619sh						616	γC2–H8, γC3–H9		
569s	570w	591	τwCH$_2$(C16), δ_C11C5C6			564	γC6–C13	565	δ_C11C5C6
									γC6–C13
569s	570w	559	βR$_2$, γC6–C13	555	γC6–C13				
542sh	540w			539	γC11–C16	537	βR$_2$		
534w		534	δ_C3C4O23	534	δ_C3C4O23			531	βR$_2$
499w	496sh	519	γC11–C16	498	δ_C16C11C19, βR$_3$				
	484w							486	δ_C3C4O23
478w		469	δ_C16C11C19			478	τR$_3$, δ_C3C4O23	461	δ_C16C11C19
447w	449w			455	δ_C16C11C19	444	βR$_3$		
418w	427w			433	βC6–C13, δ_C5C4O23				
						419	γC11–C16, δ_C5C4O23	419	γC11–C16 δ_C5C4O23
406w		402	βR$_3$	409	βR$_3$, ρC11–C5			405	βR$_3$
400sh	396w	395	βC6–C13, δ_C5C4O23			389	δ_C16C11C19		
	367 m	351	ρC11–C5			359	ρC11–C5	351	βC6–C13
	333w	338	τR$_1$	344	βC6–C13, δ_C5C4O23				
	324w			315	τR$_1$				
	311w					308	τR$_1$	310	τR$_1$
	295sh	269	τOH	274	βR$_2$	283	δ_C3C4O23	288	ρC11–C5
	241vw	263	τR$_3$, τR$_1$	243	τOH			234	τOH
	218sh			220	τwCH$_3$	228	τOH		
	203sh					199	δ_C11C5C4	197	τwCH$_3$
		185	δ_C11C5C4	190	δ_C11C5C4			193	δ_C11C5C4
	178 m	172	τwCH$_3$	171	δ_C11C5C6	171	τwCH$_3$	173	δ_C11C5C6 δ_C11C5C4
	132s	156	δ_C11C5C6			159	δ_C11C5C6		
	132s	112	τR$_3$			119	τR$_2$	121	τR$_2$
	104s	90	τR$_2$	101	τR$_2$	103	τR$_3$	98	τR$_3$
	84sh			83	τR$_3$				
	73vs	50	τwC11–C5	61	τwC11–C5				
						35	τwC11–C5	37	τwC11–C5

Abbreviations: ν, stretching; wag, wagging; τ, torsion; ρ, rocking; τw, twisting; δ, deformation; a, antisymmetric; s, symmetric.
[a] This work.
[b] From scaled quantum mechanics force field B3LYP/6-31G* method.

Table 4
Comparison of scaled internal force constants for the most stable C1-1 and C1-2 conformers of (4*R*,5*R*)-carquejol, and C3-1 and C3-2 conformers of (4*S*,5*R*)-carquejol compared with those reported for other terpenes.

B3LYP Method									
Force constant	C1-1[a]		C1-2[a]		C3-1/C3-2[a]		B3LYP 6-31G*		
	6-31G*	6-311++G**	6-31G*	6-311++G**	6-31G*	6-311++G**	Cnicin[b]	Epi[c]	Onopor[d]
f(νO–H)	7.10	7.50	7.20	7.50	7.20/7.20	7.60/7.60	6.99	6.92	7.16
f(νC–H)	4.82	5.02	4.80	4.60	4.80/4.82	4.77/4.82			4.96
f(ν=CH$_2$)	5.16	5.08	5.16	5.08	5.19/5.15	5.10/5.07	5.22	5.20	
f(νCH$_2$)	4.67	4.62	4.80	4.58	4.67/4.64	4.61/4.60	4.79	4.74	4.90
f(νC–O)$_c$	4.60	4.30	4.70	4.50	4.80/4.70	4.50/4.50	5.44	4.47	4.80
f(νC–C)	4.92	4.85	4.92	4.82	4.87/4.87	4.80/4.78			
f(δ=CH$_2$)	0.40	0.40	0.40	0.40	0.40/0.40	0.40/0.40	0.44	0.43	0.45
f(δCH$_2$)	0.80	0.80	0.80	0.80	0.80/0.80	0.80/0.80	0.76	0.76	0.77
f(δC–OH)	0.70	0.70	0.70	0.70	0.70/0.70	0.70/0.70			0.74

Units are mdyn Å^{-1} for stretching and mdyn Å rad^{-2} for angle deformations.
[a] This work.
[b] From Ref. [27].
[c] From Ref. [28].
[d] From Ref. [47].

to the other terpenes, and, besides the similarity in their force constants could probably explain the potential pharmacological properties observed in carquejol because the three terpenes used for comparison exhibit several biological activities and slightly higher force constants values.

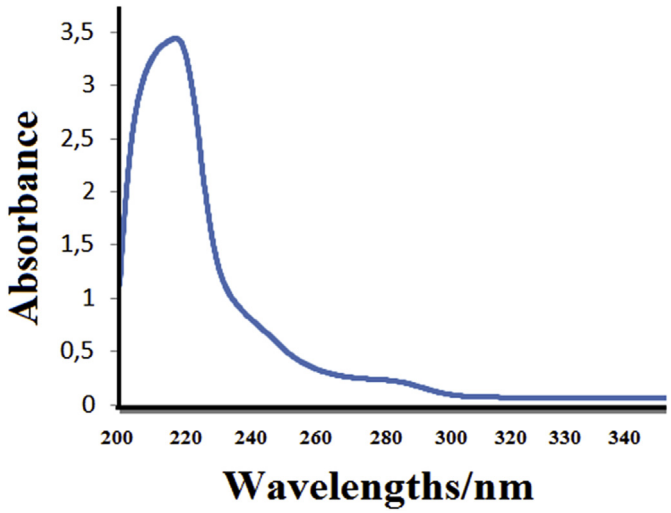

Fig. 7. Experimental Ultraviolet–visible spectrum of carquejol in ethanol 96°.

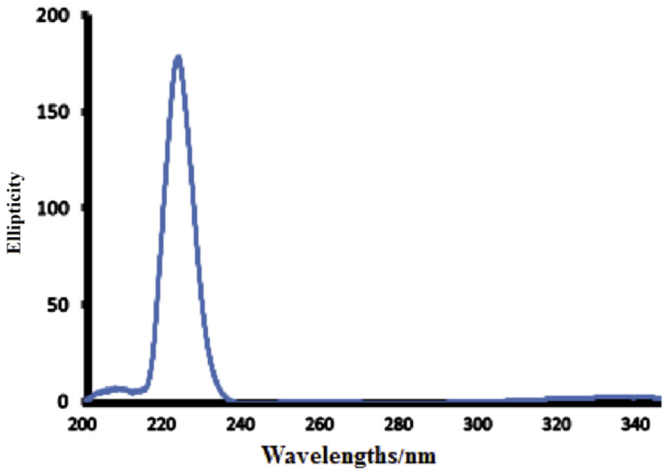

Fig. 8. Experimental electronic circular dichroism spectrum of carquejol in ethanol 96°.

6. Ultraviolet–visible spectrum

The electronic spectra for all structures of carquejol were predicted in water at the B3LYP/6-31G* level of theory. All predicted spectra are compared in Fig. S14. The experimental spectrum in ethanol 96° showed a single intense absorption at 216.6 nm (Fig. 7) while in n-hexane the maximum appeared at 208 nm. The observed hypsochromic shift is in agreement with the change in solvent polarity. Due to the presence of three C=C double bonds this absorption can be quickly assigned to $\pi \rightarrow \pi^*$ transitions, as reported for compounds with C=C bonds [28,51]. The predicted UV spectra can be seen in Fig. S14. No significant differences are observed in these spectra in relation to the experimental one.

7. Electronic circular dichroism (ECD)

The experimental ECD spectrum of carquejol recorded in the 200–400 nm regions is observed in Fig. 8. Usually, the ECD spectrum shows the three-dimensional arrangement of the C=C chromophore groups in carquejol [52]. We observed a strong positive band at 223.6 nm (Fig. 8) that can be easily assigned to the $\pi \rightarrow \pi^*$ transitions usually observed between 210 and 220 nm which involve the C=C groups. Here, the excitation energies, and their corresponding oscillator strength and rotatory strength can be easily obtained from the TD-DFT calculations. When the oscillator strengths are graphed versus the wavelengths we observed similar spectra for all conformers but, when the rotatory strengths were represented in function of wavelengths we observed that the predicted ECD spectrum for C3-1 is similar to the experimental one. This way we can confirm that the (4S,5R) structure corresponding to that theoretical C3-1 is present in agreement with the result obtained by Snatzke et al. [13].

8. Conclusions

In the present work, carquejol was prepared from carquejyl acetate, the major component of the essential oil from *B. trimera*. The natural alcohol was characterized by FTIR and Raman, UV–Visible, ECD, Mass, ^{1}H and ^{13}C NMR and 2D ^{1}H–^{1}H gCOSY, ^{1}H-^{13}CgHSQC, ^{1}H-^{13}CgHMBC spectroscopies. Theoretically, the four possible (4*R*,5*R*), (4*S*,5*R*), (4*R*,5*S*) and (4*S*,5*S*) stereoisomes of carquejol named C1, C3, C4 and C5 respectively were considered and, since C1/C5 and C3/C4 are enantiomeric pairs, only diastereomers C1 and C3 were analysed as they are energetically identical to C5 and C4 respectively. Thus, two stable conformations were found for both distereomers: C1-1 and C1-2 for the non-natural (4*R*,5*R*)-carquejol, and C-3-1 and C3-2 for the natural (4*S*,5*R*)-isomer. The potential energy surface with minima energies and different populations by using the hybrid B3LYP method with the 6-31G* and 6-311++G** basis sets are presented. The different orientations and directions of the corresponding dipole moments could probably justify their reactivities and behaviour in different media. The differences between the dipole moments are justified by the MK charges. The studies by using the MEP surfaces for all structures have shown that the nucleophilic and electrophilic sites of higher reactivity are principally those centred on the OH groups. The NBO studies suggest higher stabilities for C1-1 and C1-2 while the AIM analyses support the high stabilities of C3-1 and C3-2. The studies by using the frontier orbitals reveal that carquejol has a lower reactivity when compared with other terpenes while the similarity among the nucleophilicity indexes with other terpenes could explain their biological activities. A good concordance was found among the experimental FTIR, FT-Raman, UV–Visible and ^{1}H and ^{13}C NMR spectra and their corresponding theoretical ones. The predicted ECD spectrum for C3-1 conformer is similar to the experimental one. Here, the SQMFF force fields for all conformers by using the two levels of theory were reported and the complete vibrational assignments of the 69 normal vibration modes for both conformers of carquejol were presented. Finally, the force constants for all species were also reported and compared with the corresponding to known terpenes.

Acknowledgements

This work was supported with grants from CIUNT Project N° 26/D207 (Consejo de Investigaciones, Universidad Nacional de Tucumán) and CONICET (Consejo Nacional de Investigaciones Científicas y Técnicas, R. Argentina). MM thanks Agencia Nacional de Investigación e Innovación (ANII-Uruguay) for PhD grants (POS 2011 1 3332 and POS NAC 2013 1 11316) and Universidad Nacional de Tucumán (PEEP Program). The authors would like to thank Prof. Tom Sundius for his permission to use MOLVIB.

Appendix A. Supplementary data

Supplementary data related to this article can be found at http://dx.doi.org/10.1016/j.molstruc.2017.08.068.

References

[1] L.M.B. Torres, M.T. Gamberini, N.F. Roque, M.T.L. Landman, C. Souccar, A.J. Lapa, Diterpene from *Baccharistrimera* with a relaxant effect on rat vascular smooth muscle, Phytochemistry 55 (2000) 617–619.

[2] O. Hnatyszyn, V. Moscatelli, J. Garcia, R. Rondina, M. Costa, C. Arranz, A. Balaszczuk, G. Ferraro, J.D. Coussio, Argentinian plant extracts with relaxant effect on the smooth muscle of the *corpus cavernosum* of Guinea pig, Phytomedicine 10 (2003) 669–674.

[3] R.M. Gené, C. Cartañá, T. Adzet, E. Marin, T. Parella, S. Cañigueral, Anti-inflammatory and analgesic activity of *Baccharistrimera*: identification of its active constituents, PlantaMedica 62 (1996) 232–235.

[4] A.H. Januário, S.L. Santos, S. Marcussi, M.V. Mazzi, R.C.L.R. Pietro, D.N. Sato, J. Ellena, S.V. Sampaio, S.C. Franc, A.M. Soares, Neo-clerodanediterpenoid, a new metalloprotease snake venom inhibitor from *Baccharistrimera*(Asteraceae): anti-proteolytic and anti-hemorrhagic properties, Chem. Biol. Interact. 150 (2004) 243–251.

[5] F.A. de Oliveira Garcia, M.M. Tanae, L.M. Brandão Torres, A.J. Lapa, M.T.R. de Lima-Landman, C. Souccar, A comparative study of two clerodanediterpenes from *Baccharistrimera* (Less.) DC. on the influx and mobilization of intracellular calcium in rat cardiomyocytes, Phytomedicine 21 (2014) 1021–1025.

[6] C.A. Caneschi, F.J. Martins, D.G. Larrudé, E.C. Romani, M.A.F. Brandão, N.R.B. Raposo, *In vitro* antifungal activity of *Baccharistrimera* Less (DC) essential oil against Dermatophytes, Trop. J. Pharm. Res. 14 (11) (November 2015) 2083–2089.

[7] C.A. Simões-Pires, S. Debenedetti, E. Spegazzini, L.A. Mentz, N.I. Matzenbacher, R.P. Limberger, A.T. Henriques, Investigation of the essential oil from eight species of Baccharis belonging to sect. Caulopterae (Asteraceae, Astereae): a taxonomic approach, Pl. Syst. Evol. 253 (2005) 23–32.

[8] C.A. Simões-Pires, E.F. Queiroz, A.T. Henriques, K. Hostettmann, Isolation and on-line identification of antioxidant compounds from three Baccharis species by HPLC–UV–MS/MS with post-column derivatisation, Phytochem. Anal. 16 (2005) 307–314.

[9] M.P. Sousa, M.E.O. Matos, F.J.A. Matos, M.I.L. Machado, A.A. Craveiro, Carqueja, in: M.P. De Sousa, et al. (Eds.), Constituintes Químicos Ativos de Plantas Medicinais Brasileiras, UFC, Fortaleza, 1991, pp. 223–228.

[10] J.C. Borella, D.P. Duarte, A.A.G. Novaretti, A. Menezes Jr., S.C. França, C.B. Rufato, P.A.S. Santos, R.C.S. Veneziani, N.P. Lopes, Variabilidadesazonal do teor de saponinas de Baccharistrimera (Less) DC (Carqueja) e isolamento de flavona, Rev. Bras. Farmacogn. 16 (2006) 557–561.

[11] R.N. de Oliveira, V.L.G. Rehder, A.S. Santos Oliveira, I. Montanari Jr., J.E. de Carvalho, A.L.T. G. de Ruiz, V.L.S. Jeraldo, A.X. Linhares, S.M. Allegretti, Schistosomamansoni: in vitro schistosomicidalactivity of essential oil of Baccharistrimera (Less.) DC, Exp. Parasitol. 132 (2012) 135–143.

[12] F.G. Silva, C.B.A. Oliveira, J.E.B.P. Pinto, V.E. Nascimento, S.C. Santos, J.C. Seraphin, P.H. Ferri, Seasonal variability in the essential oils of wild and cultivated baccharistrimera, J. Braz. Chem. Soc. 18 (5) (2007) 990–997.

[13] G. Snatzke, A.F. Thomas, G. Ohloff, Die absolute Konfiguration von Carquejol und verwandten *0*-Menthan-Derivaten, Helvetica Chim. Acta 52 (5) (1969) 1253–1258.

[14] A.D. Becke, Density-functional exchange-energy approximation with correct asymptotic behavior, Phys. Rev. A38 (1988) 3098–3100.

[15] C. Lee, W. Yang, R.G. Parr, Development of the Colle-Salvetti correlation-energy formula into a functional of the electron density, Phys. Rev. B 37 (1988) 785–789.

[16] E.D. Glendening, J.K. Badenhoop, A.D. Reed, J.E. Carpenter, F. Weinhold, NBO 3.1; Theoretical Chemistry Institute, University of Wisconsin, Madison, WI, 1996.

[17] R.F.W. Bader, Atoms in Molecules. A Quantum Theory, Oxford University Press, Oxford, 1990, ISBN 0198558651.

[18] F. Biegler-Köning, J. Schönbohm, D. Bayles, AIM2000; a program to analyze and visualize atoms in molecules, J. Comput. Chem. 22 (2001) 545.

[19] a) G. Rauhut, P. Pulay, Transferable scaling factors for density functional derived vibrational force fields, J. Phys. Chem. 99 (1995) 3093–3099;
b) G. Rauhut, P. Pulay, J. Phys. Chem. 99 (1995) 14572.

[20] T. Sundius, Scaling of ab initio force fields by MOLVIB, Vib. Spectrosc. 29 (2002) 89–95.

[21] R.G. Parr, R.G. Pearson, Absolute hardness: companion parameter to absolute electronegativity, J. Am. Chem. Soc. 105 (1983) 7512–7516.

[22] M.B. Márquez, S.A. Brandán, A structural and vibrational investigation on the antiviral Deoxyribonucleoside thymidine agent in gas and aqueous solution phases, Int. J. Quantum Chem. 114 (2014) 209–221.

[23] A.B. Raschi, E. Romano, M.V. Castillo, P. Leyton, C. Paipa, L.M. Maldonado, S.A. Brandán, Vib. Spectrosc. 70 (2014) 100–109.

[24] D. Romani, S.A. Brandán, Structural and spectroscopic studies of two 1,3-benzothiazole tautomers with potential antimicrobial activity in different media. Prediction of their reactivities, Comput. Theoret. Chem. (Theochem) 1061 (2015) 89–99.

[25] Jean-Luc Bredas, Mind the gap!, Mater. Horiz. 1 (2014) 17–19.

[26] F. Chain, M.F. Ladetto, A. Grau, C.A.N. Catalán, S.A. Brandán, Structural, electronic, topological and vibrational properties of a series of N-benzylamides derived from Maca (Lepidiummeyenii) combining spectroscopic studies with ONION calculations, J. Mol. Struct. 1105 (2016) 403–414.

[27] F. Chain, E. Romano, P. Leyton, C. Paipa, C.A.N. Catalán, M.A. Fortuna, S.A. Brandán, An experimental study of the structural and vibrational properties of sesquiterpene lactone cnicin using FT-IR, FT-Raman, UV–visible and NMR spectroscopies, J. Mol. Struct. 1065–1066 (2014) 160–169.

[28] F.E. Chain, P. Leyton, C. Paipa, M. Fortuna, S.A. Brandán, FT-IR, FT-Raman, UV-Visible, and NMR spectroscopy and vibrational properties of the labdane-type diterpene 13-epi-sclareol, Spectrochim. Acta Part A 138 (2015) 303–313.

[29] D. Romani, S.A. Brandán, Effect of the side chain on the properties from cidofovir to brincidofovir, an experimental antiviral drug against to *Ebola* virus disease, Arab. J. Chem. (2015), http://dx.doi.org/10.1016/j.arabjc.2015.06.030. In Press.

[30] V. Theodorou, K. Skobridis, A.G. Tzakos, V. Ragoussis, A simple method for the alkaline hydrolysis of esters, Tetrahedron Lett. 48 (2007) 8230–8233.

[31] a) F. Caujolle, D. Meynier, J. Cros, Pharmacological study of carquejol and its derivatives, Therapie 15 (1960) 931–939;
b) F. Caujolle, D. Meynier, Pham-Huu-Chanh, toxicity of carquejol, Ann. Pharm. Fr. 18 (1960) 715–725.

[32] Y.R. Naves, F. Caujolle, U.S. Patent 3,112 (1963) 245.

[33] A.B. Nielsen, A.J. Holder, Gauss View 5.0, User's Reference, GAUSSIAN Inc., Pittsburgh, PA, 2008.

[34] M.J. Frisch, G. W. Trucks, H.B. Schlegel, G.E. Scuseria, M.A. Robb, J.R. Cheeseman, G. Scalmani, V. Barone, B. Mennucci, G.A. Petersson, H. Nakatsuji, M. Caricato, X. Li, H.P. Hratchian, A.F. Izmaylov, J. Bloino, G. Zheng, J.L. Sonnenberg, M. Hada, M. Ehara, K. Toyota, R. Fukuda, J. Hasegawa, M. Ishida, T. Nakajima, Y. Honda, O. Kitao, H. Nakai, T. Vreven, J.A. Montgomery, Jr, J.E. Peralta, F. Ogliaro, M. Bearpark, J.J. Heyd, E. Brothers, K. N. Kudin, V.N. Staroverov, R. Kobayashi, J. Normand, K. Raghavachari, A. Rendell, J.C. Burant, S.S. Iyengar, J. Tomasi, M. Cossi, N. Rega, J.M. Millam, M. Klene, J.E. Knox, J.B. Cross, V. Bakken, C. Adamo, J. Jaramillo, R. Gomperts, R.E. Stratmann, O. Yazyev, A.J. Austin, R. Cammi, C. Pomelli, J.W. Ochterski, R.L. Martin, K. Morokuma, V.G. Zakrzewski, G.A. Voth, P. Salvador, J.J. Dannenberg, S. Dapprich, A.D. Daniels, O. Farkas, J.B. Foresman, J.V. Ortiz, J. Cioslowski, and D.J. Fox, Gaussian, Inc., Wallingford CT, 2009.

[35] B.H. Besler, K.M. Merz Jr., P.A. Kollman, Atomic charges derived from semi-empirical methods, J. Comp. Chem. 11 (1990) 431–439.

[36] R. Ditchfield, Self-consistent perturbation theory of diamagnetism. I. A gage-invariant LCAO (linear combination of atomic orbitals) method for NMR chemical shifts, Mol. Phys. 27 (1974) 714–722.

[37] E. Romano, A.B. Raschi, A.M. Benavente, S.A. Brandán, Structural analysis, vibracional spectra and coordinated normal of 2R-(_)-6-hydroxytremetone, Spectrochim. Acta Part A Mol. Biomol. Spectrosc. 84 (2011) 111–116.

[38] E. Romano, M.V. Castillo, J. Pergomet, J. Zinczuk, S.A. Brandán, Synthesis, structural study and spectroscopic characterization of a Quinolin-8-Yloxy derivative with potential biological properties, Open J. Synth. Theor. Appl. 2 (2013) 8–22.

[39] E. Romano, F. Ladetto, S.A. Brandán, Structural and vibrational studies of the potential anticancer agent, 5-difluoromethyl-1,3,4-thiadiazole-2-amino by DFT calculations, Comput. Theor. Chem. 1011 (2013) 57–64.

[40] K. Guzzetti, A.B. Brizuela, E. Romano, S.A. Brandán, Structural and vibrational study on zwitterions of L-threonine in aqueous phase using the FT-Raman and SCRF calculations, J. Molec. Struct. 1045 (2013) 171–179.

[41] I. Caracelli, J. Iulek, A. Neves, I. Vencato, F. Silva Jnr, T.J. Brocksom, J. Zukerman-Schpector, Intermediates in the synthesis of cembrane diterpenes, Acta Cryst. C53 (1997) 1282–1284.

[42] I. Rodríguez-Escudero, J. Marrero, A.D. Rodríguez, Kallolide A acetatepyrazoline, Acta Cryst. E68 (2012) o41–o42.

[43] L. Tapia, J. Torres, L. Mendoza, A. Urzúa, J. Ferreira, M. Pavani, M. Wilkens, Effect of 13-epi-sclareol on the bacterial respiratory chain, Planta Med. 70 (11) (2004) 1058–1063.

[44] K.V. Sashidhara, J.N. Rosaiah, A. Kumar, H.K. Bid, R. Konwar, N. Chattopadhyay, Cell growth inhibitory action of an unusual labdane diterpene, 13-epi-sclareol in breast and uterine cancers in Vitro, Phytothrer Res. 21 (11) (2007) 1105–1108.

[45] A. Urzúa, M.C. Rezende, C. Mascayano, L. Vásquez, A structure-activity study of antibacterial diterpenoids, Molecules 13 (2008) 882–891.

[46] Y. Wang, W.-N. Wu, R.-Q. Zhao, A.-Y. Zhang, B.-F. Qin, Acta Cryst. E66 (2010) m292.

[47] F. Chain, E. Romano, P. Leyton, C. Paipa, C.A.N. Catalán, M.A. Fortuna, S.A. Brandán, Vibrational and structural study of onopordopicrin based on the FTIR spectrum and DFT calculations, Spectrochim. Acta 150 (2015) 381–389.

[48] G. Keresztury, S. Holly, G. Besenyei, J. Varga, A.Y. Wang, J.R. Durig, Vibrational spectra of monothiocarbamates-II. IR and Raman spectra, vibrational assignment, conformational analysis and *ab initio* calculations of *S*-methyl-*N,N*-dimethylthiocarbamate, Spectrochim. Acta 49A (1993) 2007–2026.

[49] D. Michalska, R. Wysokinski, The prediction of Raman spectra of platinum(II) anticancer drugs by density functional theory, Chem. Phys. Lett. 403 (2005).

[50] C.H. Görbitz, W.H. Nelson, E. Sagstuen, Acta Crystallogr. E61 (2005) o1207.

[51] T.J. Bruno, P.D.N. Svoronos, CRC Handbook of Basic Tables for Chemical Analysis, second ed., CRC Press, Taylor & Francis Goup, Boca Raton, 2011.

[52] A.E. Nugroho, H. Morita, Circular dichroism calculation for natural products, J. Nat. Med. 68 (2014) 1–10.